Taylor & Francis
Taylor & Francis Group

INVITED ARTICLE

A thermodynamic description of the adsorption-induced structural transitions in flexible MIL-53 metal-organic framework

François-Xavier Coudert[a,*], Anne Boutin[b] and Alain H. Fuchs[a,*]

aInstitut de Recherche de Chimie Paris, CNRS – Chimie ParisTech, Paris, France; bDépartement de Chimie, École Normale Supérieure, CNRS-ENS- UPMC, Paris, France

We briefly review the concept of temperature-loading phase diagram that we derived from an osmotic statistical ensemble analysis of the adsorption-induced structural transitions observed in the MIL-53 family of metal-organic framework nanoporous materials. We highlight the generic nature of this diagram and comment on the occurrence of breathing transitions depending on the guest fluid, the framework functionalisation and the nature of the metal centre.

Keywords: adsorption; statistical thermodynamics; structural transitions; nanoporous materials

1. Introduction

Among the wide class of metal-organic frameworks and other related open framework hybrid materials, the subclass of soft porous crystals (SPCs) has attracted a lot of attention in the past few years. According to Kitagawa, who introduced this notion, 'soft porous crystal are defined as porous solids that possess both a highly ordered network and structural transformability. They are bistable or multistable crystalline materials with long range structural ordering, a reversible transformability between states and permanent porosity' [1]. It has been recently shown that the 'softness' of these materials, which was somewhat ill defined up to now, actually stems from a highly anisotropic mechanical (or elastic) behaviour, with some directions of the crystal exhibiting very low Young's modulus and shear modulus [2].

SPCs exhibit large-amplitude structural deformations induced by various external stimuli such as temperature, mechanical pressure or guest adsorption. Guest-induced structural transitions include the *gate adsorption* and the *breathing* phenomena. Gate adsorption typically involves an abrupt structural transition between a nonporous state and a porous crystalline host that is induced by gas adsorption [3,4]. The breathing phenomenon consists of two successive adsorption-induced crystal-to-crystal transformations, from a large pore (**lp**) state to a narrow pore (**np**) state and back again to the **lp** structure [5,6].

In a series of articles, the present authors have investigated the equilibrium thermodynamics of adsorption-induced and pressure-induced breathing transitions using an analytical approach based on the osmotic statistical ensemble. Some key questions were answered, such as the prediction of the occurrence or absence of guest-induced breathing for a given guest–host system [7–9] and the successful derivation of a {temperature–gas pressure} phase diagram for the several gases (xenon, methane and carbon dioxide)/MIL-53 systems [10–12] as well as breathing phase diagram for binary mixtures of methane and carbon dioxide/MIL-53 [13]. The physical mechanism of the breathing transitions was addressed by viewing the adsorption-induced stress exerted on the material as the stimulus that triggers breathing transitions, in a way similar to **lp**-to-**np** structural transitions that can be induced by mechanical compression. This new view of the breathing that we proposed implies that the structural transitions in SPCs take place when the stress reaches a certain critical threshold [14,15]. Though the exact chemical origins of this stress have not yet been fully uncovered, it is similar in nature to the elastic limit (or yield strength) in classical mechanics, where the deformation stops being quasistatic. For example, a recent molecular simulation study has shed some light on the pressure-induced amorphisation of Zeolitic Imidazolate Framework ZIF-8 [16]: the amorphisation transition in this material was shown to be the result of pressure-induced softening, until the pressure reached a value at which the crystal was not mechanically stable (Born's stability criteria no longer hold). Although it has not been equivocally demonstrated, we envision that a similar mechanism might be in play in the breathing of MIL-53.

This hypothesis of a 'critical stress threshold' enabled to explain, at least qualitatively, the hysteresis phenomenon observed in the breathing transitions; when approaching the

---

*Corresponding authors. Email: fx.coudert@chimie-paristech.fr and alain.fuchs@cnrs-dir.fr

structural transition, the material is in two different phases on the adsorption and desorption branches, whose critical stress need not be equal (it was demonstrated, for example, that other mechanical properties such as the bulk modulus vary between the two phases [15]). Moreover, this concept was used as a basis for building a multiscale dynamic model in order to capture the dynamics of adsorption-induced deformation and structural transformation in MIL-53 based on the coupling of the host–guest adsorption interactions with the elastic response of the three-dimensional framework of a given geometry [17,18]. Finally, the issue of multistability and intermediate structures was recently addressed, using the osmotic potential approach [19].

In this paper, we briefly review the equilibrium temperature-loading phase diagrams (i.e. the {temperature– gas pressure} diagrams) that were computed for different guest-MIL-53 systems. We highlight the generic nature of this diagram and comment on the occurrence of breathing transitions depending on the guest fluid, the framework functionalisation and the nature of the metal centre.

2. Temperature-loading diagrams for several guest-MIL-53(Al) systems

We have used a model based on the so-called osmotic ensemble [7], which is the appropriate statistical ensemble to describe fluid adsorption in a flexible porous material. Since the MIL-53 material exhibits clear structural transitions between two metastable framework structures, namely the 'narrow pore', **np** phase, and the 'large pore', **lp** phase (see Figure 1), we were able to use a simplified *osmotic sub-ensemble* to describe the equilibrium between host structures upon fluid adsorption [7,8]. Langmuir fits of the experimental isotherms served as approximations to the rigid host isotherms in both the **lp** and **np** structures. We showed that, at a fixed temperature, the occurrence of breathing (or other structure transitions) upon adsorption could be rationalised by three key parameters with clear physical meaning: the affinity of the fluid for each phase (as described by the Langmuir's Henry constant), the capacity (or saturation uptake) of fluid in each phase and the free energy difference between the empty phases.

In the first study of this series, performed on the {Xenon- MIL-53 (Al)} system [10], we have used stepped isotherms at two temperatures to determine the transition enthalpy and entropy of the empty host material, as well as the free energy difference between the empty **lp** and the **np** structures. Not unexpectedly, the **lp** form was predicted to be the most stable one at room temperature, while the **np** structure becomes the most stable one below 203 K. One of the interests of the osmotic thermodynamic model is that it enables to compute equilibrium thermodynamic data for the bare host material using thermodynamic adsorption data only.

The osmotic model, with the use of the fits performed on the experimental adsorption isotherms, enables to in-
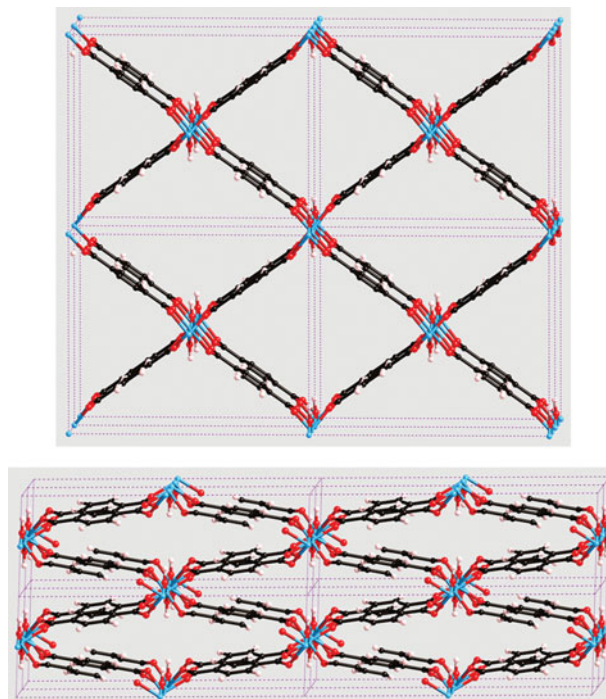

Figure 1. Representation of the metastable **lp** (top) and **np** (bottom) structures of the MIL-53(Al) material, as a $2 \times 2 \times 2$ supercell viewed along the axis of the unidimensional channels.

vestigate the full temperature-loading phase diagram of {Xe, MIL-53(Al)}. By solving the osmotic thermodynamic equations numerically, we determined for each temperature whether breathing takes place and if so, what the transition pressures are. The predicted temperature–xenon gas pressure diagram is shown in Figure 2.

The **lp** phase was found to be stable at high temperature and again at lower temperature. There is an intermediate **np** phase stability domain for xenon pressure lower than a limiting pressure of around 1.6 bar. This result is reminiscent of the re-entrant behaviour observed in some liquid crystals [20]. As noted above, however, the low-temperature
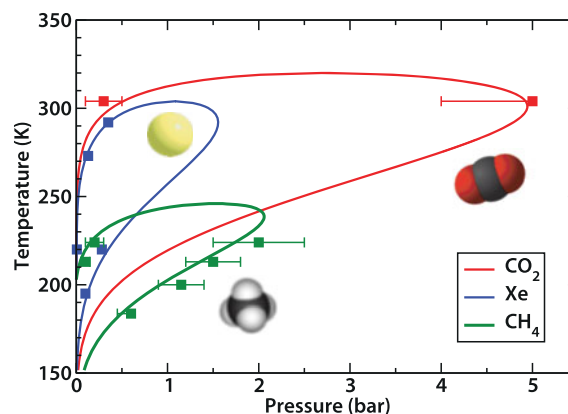

Figure 2. Comparison of the temperature–gas pressure phase diagrams for CO_2 (red), CH_4 (green) and Xe (blue) adsorption in MIL-53 (Al) [12]. Experimental transition pressures are indicated by square symbols.
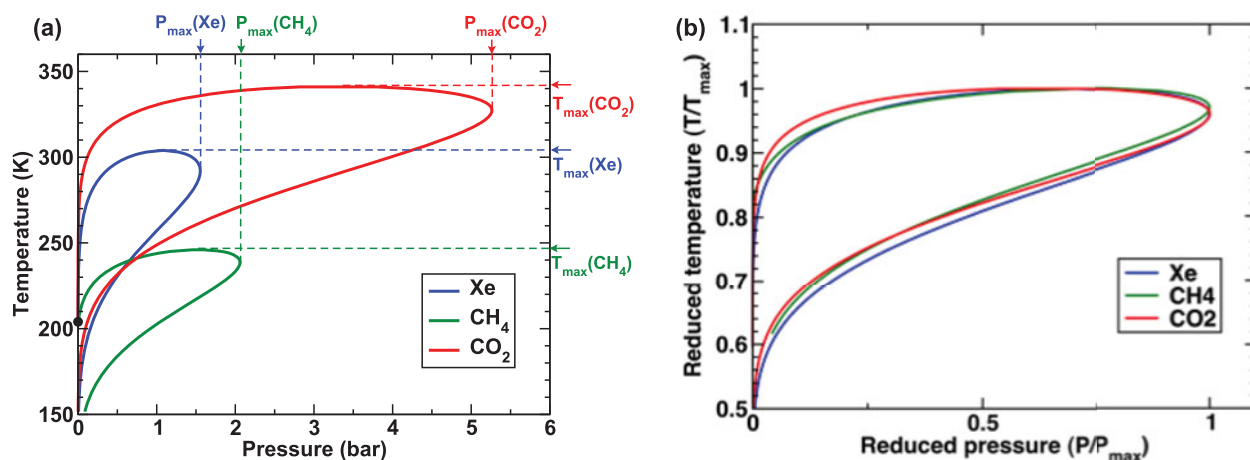
Figure 3.   Left: comparison of the temperature–vapour pressure phase diagrams for CO_2 (red), CH_4 (green) and Xe (blue) adsorption in MIL-53(Al), with the extremal temperatures and pressures marked. Right: same three phase diagrams in reduced units of (T/T_{max}) and (P/P_{max}). Left figure is reproduced with permission from [12], © 2010 American Chemical Society.

stable phase at zero pressure (empty material) is the **np** phase.

The phase diagrams for the {CO_2, MIL-53(Al)} and {CH_4, MIL-53(Al)} are also shown in Figure 2 [12]. All three diagrams have in common the equilibrium **np–lp** temperature T_0 of 203 K at zero pressure. The initial slope of the transition curve is proportional to the logarithm of (K_{np}/K_{lp}), the ratio of adsorption affinities in the two structures, and is thus strictly positive since the affinity of the guest adsorbate for the closed form of the framework is higher than for the open form [7,10]. The condition $K_{np}/K_{lp} > 1$ thus favours the closed **np** phase, and consequently the phase transition temperature increases with the gas loading (i.e. the stability domain of the **np** phase increases with $P_{adsorbate}$). At higher temperature, the transition free energy increases, and it becomes more and more difficult to maintain the **np** form as the most stable one. This causes the observed bending of the transition line. For obvious entropy reasons, the **lp** phase will eventually become more stable at high temperature, regardless of the gas loading. This situation is also true at high pressure. As the adsorbate pressure increases, at any temperature, the **lp** structure will eventually become more stable than the **np** one because it can accommodate a higher loading of guest molecules. Since the **lp** phase is the most stable one at high enough temperature as well as at high adsorbate pressure, one has to conclude that the stability domain of the **np** phase should be limited in adsorbate pressure ($P_{max} \sim 5$ bar in the case of carbon dioxide, 2 bar in the case of methane and 1.6 bar in the case of xenon, see Figure 2).

The above thermodynamic considerations are very general and obviously not limited to the special case of one or the other gas adsorption. The condition $K_{np}/K_{lp} > 1$ is expected to hold true for all the simple guest molecules that have been investigated so far. This means that there should be a range of temperatures above the equilibrium

np–lp transition temperature of the bare MIL-53(Al) material (203 K in our model, subject to an estimated uncertainty of ±10 K), where the initially empty open structure contracts upon guest molecule adsorption. The fact that this has not been observed in some cases at room temperature simply means that the transition line maximum in this system is below the room temperature. The present findings for methane clearly confirm these predictions.

The difference in the stability domain of the **np** phase in the three different cases can be qualitatively understood as follows. For each system, there is a temperature T_{max} (see Figure 3a), above which gas adsorption does not induce the **lp–np** phase transition anymore. Since the driving force for the closure of the **lp** structure is the guest–host interaction, which induces the cell contraction, one may simply write $k \, T_{max} \sim \Delta H_{ads,lp}$. The increase in T_{max} in going from CH_4 to Xe and CO_2 can then simply be explained by the increase in adsorption enthalpy in the **lp** phase. While P_{max} is approximately the same for CH_4 and Xe, its value for CO_2 is larger by a factor of ∼3. This difference can be accounted for by a larger interaction energy between guest molecules in the case of carbon dioxide, due to their quadrupole moments. This causes a stronger ordering of the CO_2 molecules in the **np** phase and increases the stability domain of this phase.

In Figure 3b, we sketch the three phase diagrams in reduced units of (T/T_{max}) and (P/P_{max}). Some sort of a 'universal' phase diagram seems to come out of this presentation. This confirms the existence of a *generic* temperature-loading phase diagram, as long as the adsorbate is a simple gas such as methane, carbon dioxide or xenon.

It must be recalled at this stage that the osmotic model predicts the conditions of thermodynamic stability at full equilibrium and does not take into account hysteresis effects. Hysteresis was systematically encountered in all reported MIL-53 experiments and often leads to some complicated mixtures of phases [21]. This model describes what
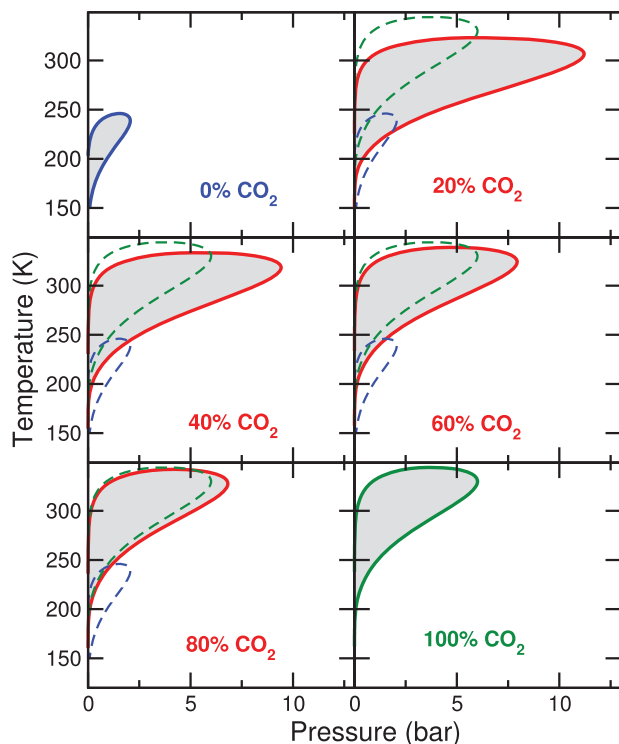
Figure 4. Temperature–pressure phase diagram of MIL-53(Al) upon adsorption of a CO_2/CH_4 mixture, with increasing CO_2 molar fraction. Dashed lines correspond to pure component diagrams: CO_2 in green, CH_4 in blue. Reproduced with permission from [13], © 2011 American Chemical Society.

Figure 5. Temperature–CO_2 pressure phase diagrams for regular MIL-53(Al) (red) and amino-MIL-53(Al) (blue) materials. The T_0 are the equilibrium phase transition temperature between the **lp** and **np** phases at zero pressure (i.e. the empty material) for both materials. Modified with permission from [11], © 2010 Elsevier Inc.

would happen in a homogeneous system at full equilibrium. The osmotic model is aimed at describing the thermodynamics behind the scene. The hysteresis issue is being addressed in some of our other studies [14–19].

Finally, one should mention that the osmotic model was extended to predict the behaviour of fluid mixtures adsorbing in flexible nanoporous materials by proposing an analytical scheme called OFAST (osmotic framework adsorbed solution theory) [13]. Figure 4 represents the $\{CO_2/CH_4,$ MIL-53(Al)$\}$ diagrams for different values of the carbon dioxide mole fraction. We can see that, in addition to the re-entrant nature of the phase diagrams themselves in (T, P) space, there is a nonmonotonic evolution of the maximal temperature and pressure of the **np** phase as a function of the mixture's composition. This unexpected result, first hypothesised on a purely theoretical thermodynamic basis [9], was later proven true by experimental measurements [13].

3. Temperature-loading phase diagrams for some other guest-MIL-53 materials systems

The osmotic temperature-loading phase diagram can be used to study the effect of changes in the material's composition on the breathing behaviour. We have performed an
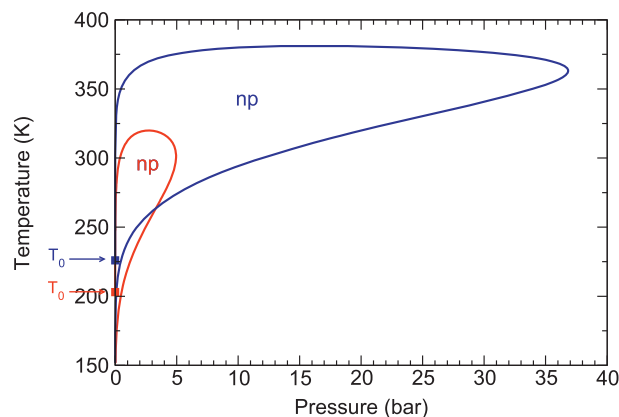
experimental and theoretical study of carbon dioxide adsorption in amino-functionalised MIL-53(Al), jointly with the group of Denayer [11]. In Figure 5, the $\{CO_2,$ amino-MIL-53(Al)$\}$ diagram is compared with the "regular" MIL-53(Al) diagram. The equilibrium **np–lp** temperature T_0 is slightly different (203 K for regular MIL-53 and 226 K for amino-MIL-53), and the initial slope of the transition line is higher in the case of the amino-MIL system. Even though the overall shape of the temperature–gas pressure phase diagram is similar, there is a spectacular difference in the stability domain of the **np** structure, which can be accounted for by the increased stability of this form due to the presence of the amino groups in the structure. The strong affinity of CO2 molecules in the **np** form leads to a larger value of K_{np}/K_{lp} for the amino-MIL material compared to the regular MIL-53(Al) and enlarges the stability domain of the **np** form.

An even more drastic change in the MIL-53 composition consists of replacing the aluminium centre by a gallium atom. MIL-53 (Ga) was synthesised and characterised by the group of Férey [22] and then further investigated by Boutin and co-workers [23]. Breathing transitions were found to take place upon several gas adsorptions [22] but the stable phase at room temperature was found to be the **np** narrow pore structure [22,23]. A recent quantum chemistry investigation by Coudert and co-workers allowed to understand that **np** phase was more stable in the case of MIL-53 (Ga), because of the more diffuse orbitals of Ga compared to Al [24]. Thus, the **np** phase is the stable structure at room temperature (rather than **lp** as Al-MIL53). The effect of replacing Al by Ga is simply to increase the value of T_0, the **np–lp** equilibrium phase transition temperature of the empty MIL-53 framework. The whole temperature-loading phase diagram is thus switched to higher temperature.

4. Conclusion

The temperature-loading phase diagram of the flexible MIL-53 family of materials is a useful tool to understand the behaviour of adsorption-induced breathing structural transitions. Whether or not these transitions take place upon adsorption of a particular gas or gas mixture depend on the relative location of the stability regions of the **np** and **lp** states in the system's (T, P, x) space, where T is the temperature, P is the adsorbate gas pressure and x is a mole fraction describing the gas composition. Even though this is just an equilibrium thermodynamic view of the breathing process, which means for instance that it lacks the hysteresis effects that take place in the experiments, this temperature-loading concept has allowed to demonstrate that the breathing effect in MIL-53 is a very general phenomenon, that should be observed in some region of the (T, P) space whatever the guest molecule, since it is expected that the affinity of an adsorbate for the closed **np** form of the framework will always be higher than for the open **lp** structure. We also believe that this very general model can provide a useful tool for experimentalists to tune their experimental conditions. As such, the phase diagrams described here and the thermodynamic models developed to build them naturally complement the other approaches used in the field of flexible porous materials, namely poromechanics [25,26] (at the macroscopic scale) and atomistic molecular simulation (at the microscopic scale) [27–30]; the advantages and downsides of all three methods were recently reviewed in [31].

Acknowledgements

Funding

References

[1] S. Horike, S. Shimomura, and S. Kitagawa, Nature Chem. **1**, 695 (2009).
[2] A.U. Ortiz, A. Boutin, A.H. Fuchs, and F.-X. Coudert, Phys. Rev. Lett. **109**, 195502 (2012).
[3] D. Li and K. Kaneko, Chem. Phys. Lett. **335**, 50 (2001).
[4] R. Kitaura, K. Seki, G. Akiyama, and S. Kitagawa, Angew. Chem. Int. Ed. **42**, 428 (2003).
[5] G. Férey and C. Serre, Chem. Soc. Rev. **38**, 1380 (2009).
[6] C. Serre, F. Millange, C. Thouvenot, M. Nogues, G. Marsolier, D. Louer, and G. Férey, J. Am. Chem. Soc. **124**, 13519 (2002).
[7] F.-X. Coudert, M. Jeffroy, A.H. Fuchs, A. Boutin, and C. Mellot-Draznieks, J. Am. Chem. Soc. **130**, 14294 (2008).
[8] F.-X. Coudert, C. Mellot-Draznieks, A.H. Fuchs, and A. Boutin, J. Am. Chem. Soc. **131**, 3442 (2009).
[9] F.-X. Coudert, Phys. Chem. Chem. Phys. **12**, 10904 (2010).
[10] A. Boutin, M.-A. Springuel-Huet, A. Nossov, A. Gedeon, T. Loiseau, C. Volkringer, G. Férey, F.-X. Coudert, and A.H. Fuchs, Angew. Chem. Int. Ed. **48**, 8314 (2009).
[11] A. Boutin, S. Couck, F.-X. Coudert, P. Serra-Crespo, J. Gascon, F. Kapteijn, A.H. Fuchs, and J.F.M. Denayer, Microporous Mesoporous Mater. **140**, 108 (2011).
[12] A. Boutin, F.-X. Coudert, M.A. Springuel-Huet, A.V. Neimark, G. Férey, and A.H. Fuchs, J. Phys. Chem. C **114**, 22237 (2010).
[13] A.U. Ortiz, M.A. Springuel-Huet, F.-X. Coudert, A.H. Fuchs, and A. Boutin, Langmuir **28**, 494 (2012).
[14] A.V. Neimark, F.-X. Coudert, A. Boutin, and A.H. Fuchs, J. Phys. Chem. Lett. **1**, 445 (2010).
[15] A.V. Neimark, F.-X. Coudert, C. Triguero, A. Boutin, A.H. Fuchs, I. Beurroies, and R. Denoyel, Langmuir **27**, 4734 (2011).
[16] A.U. Ortiz, A. Boutin, A.H. Fuchs, and F.-X. Coudert, J. Phys. Chem. Lett. **4**, 1861 (2013).
[17] C. Triguero, F.-X. Coudert, A. Boutin, A.H. Fuchs, and A.V. Neimark, J. Phys. Chem. Lett. **2**, 2033 (2011).
[18] C. Triguero, F.-X. Coudert, A. Boutin, A.H. Fuchs, and A.V. Neimark, J. Chem. Phys. **137**, 18702 (2012).
[19] D. Bousquet, F.-X. Coudert, A.G.J. Fossati, A.V. Neimark, A.H. Fuchs, and A. Boutin, J. Chem. Phys. **138**, 174706 (2013).
[20] P.G. de Gennes and J. Prost, *The Physics of Liquid Crystals* (*International Series of Monographs on Physics, No 83*) (Oxford University Press, Oxford, 1993).
[21] F. Salles, A. Ghoufi, G. Maurin, R.G. Bell, C. Mellot-Draznieks, P.L. Llewellyn, C. Serre, and G. Férey, Angew. Chem. Int. Ed. **47**, 8487 (2008).
[22] C. Volkringer, T. Loiseau, N. Guillou, G. Férey, E. Elkaïm, and A. Vimont, Dalton Trans. 2241 (2009).
[23] A. Boutin, D. Bousquet, A.U. Ortiz, F.-X. Coudert, A.H. Fuchs, A. Balandras, G. Weber, I. Bezverkhyy, J.-P. Bellat, G. Ortiz, G. Chaplais, J.-L Paillaud, C. Marichal, H. Nouali, and J. Patarin, J. Phys. Chem. C **117**, 8180 (2013)
[24] F.-X. Coudert, A.U. Ortiz, V. Haigis, D. Bousquet, A.H. Fuchs, A. Ballandras, G. Weber, I. Bezverkhyy, N. Geoffroy, J.-P. Bellat, G. Ortiz, G. Chaplais, J. Patarin, and A. Boutin, J. Phys. Chem. C (unpublished).
[25] L. Brochard, M. Vandamme, and R.J.-M. Pellenq, J. Mech. Phys. Solids 60, 606 (2012).
[26] Coussy O, editor, *Mechanics and Physics of Porous Solids* (John Wiley & Sons, New York, 2010).
[27] A. Ghoufi and G.J. Maurin, Phys. Chem. C **114**, 6496 (2010).
[28] L. Chen, J.P.S. Mowat, D. Fairen-Jimenez, C.A. Morrison, S.P. Thompson, P.A. Wright, and T. Düren, J. Am. Chem. Soc. **135**, 15763 (2013).
[29] P.G. Yot, Q. Ma, J. Haines, Q. Yang, A. Ghoufi, T. Devic, C. Serre, V. Dmitriev, G. Ferey, C. Zhong, and G. Maurin, Chem. Sci. **3**, 1100 (2012).
[30] J. Zang, S. Nair, and D.S.J. Sholl, Chem. Phys. **134**, 184103 (2011).
[31] F.-X. Coudert, A. Boutin, A.H. Fuchs, and A.V. Neimark, J. Phys. Chem. Lett. **4**, 3198 (2013).